Pressure drops of air-water two-phase flows in horizontal U-bends

Hayashi, Kosuke
Kazi, Junichiro
Yoshida, Naoyuki
Tomiyama, Akio

Pressure Drops of Air-Water Two-Phase Flows in Horizontal U-Bends

Kosuke HAYASHI[a,*], Junichiro KAZI[a,b], Naoyuki YOSHIDA[a], Akio TOMIYAMA[a]

[a] *Graduate School of Engineering, Kobe University, 1-1 Rokkodai Nada Kobe Hyogo, 657-8501 Japan*
[b] *Chiyoda Corporation, 4-6-2, Minatomirai Nishi Yokohama Kanagawa, 220-8765 Japan*

Abstract

Pressure drops in horizontally aligned U-bends were measured for air-water bubbly, plug, slug and annular flows to examine the applicability of available correlations to the data. The bend disturbed the flow and induced large pressure drops not only within the bend but also in the downstream-side straight pipe. The bend pressure drop was therefore evaluated as the sum of the pressure drop caused within the bend and the extra pressure drop caused within the re-developing region in the downstream-side straight pipe. The experimental data were well correlated using the Lockhart-Martinelli method and the Chisholm correlation gives the most reasonable evaluation for the bend pressure drop among the available correlations tested. The fundamental functional form of the Chisholm correlation was therefore used to develop an empirical correlation applicable to the present data. The empirical correlation gave reasonable evaluations for the air-water two-phase flows.

Keywords: bend pressure drop, 180° return bend, Lockhart-Martinelli correlation, Chisholm correlation

1. Introduction

Accurate evaluations of pressure drops in pipelines are of great importance in various practical systems. A U-bend (straight pipes with 180° return bend) is one of the typical components of pipelines, and therefore, many studies on two-phase flows in U-bends have

*Corresponding author
Email address: hayashi@mech.kobe-u.ac.jp (Kosuke HAYASHI)

been carried out, e.g. studies on flow structures (da Silva Lima and Thome, 2012; Padilla et al., 2013; de Oliveira and Barbosa, 2014), void fractions (de Oliveira and Barbosa, 2014; de Oliveira et al., 2014; De Kerpel et al., 2014, 2016a,b), and pressure drops (Chisholm, 1980; Domanski and Hermes, 2008; Padilla et al., 2012; da Silva Lima and Thome, 2013; de Oliveira and Barbosa, 2014; de Oliveira et al., 2014).

Geary (1975) measured pressure drops in horizontal U-bends using the refrigerant R-22. The pipe diameter, D, was 11 mm and the ratio, $D_B^* = 2R_B/D$, of the bend radius of curvature, R_B, to D ranged from 2.3 to 6.6. He correlated the bend pressure drop in terms of the bend friction coefficient and the vapor dynamic pressure. The bend friction coefficient was given in terms of D_B^*, the vapor Reynolds number and the vapor quality. It should be noted that the bend pressure drop in his experiments includes the pressure drops in the bend and the frictional losses in the 18 inch-long straight pipes upstream and downstream the bend, so that the pressure drop should be regarded as the overall U-bend pressure drop. Chisholm (1980) proposed a pressure drop model for 90° bends and its modeling is based on the two-phase multiplier (Lockhart and Martinelli, 1949). The two-phase multiplier evaluated with the model agreed well with experimental data of Sekoguchi et al. (1969). The model was then extended to 180° bends in Chisholm (1983), whereas its applicability was not discussed there. Azzi et al. (2000) reviewed available bend pressure drop correlations including the Chisholm correlation (Chisholm and Sutherland, 1969; Chisholm, 1983) and some another correlations based on the two-phase multiplier. They compared the characteristics of the correlations for cases of 90° bends and concluded that the Chisholm correlation can give fairly physically reasonable evaluations. Chen et al. (2004) obtained databases of the pressure drop for R-410A in serpentine tubes consisting of several U-bends. They extended the Geary correlation by introducing the liquid Reynolds number and the Weber number into the bend friction coefficient so as to account for effects of the liquid viscosity and the surface tension. Domanski and Hermes (2008) collected the data from Geary (1975) and Chen et al. (2004) to examine the accuracy of the correlations of Geary, Chen and Chisholm (Chisholm, 1980, 1983) to the data. Comparisons of the available correlations with the collected data showed that the accuracy of them is insufficient, and

therefore, Domanski and Hermes proposed another correlation expressed as a product of the two-phase pressure drop in the straight pipe and a bend effect multiplier consisting of the vapor Reynolds number, the vapor quality, the density ratio and D_B^* to obtain better evaluations. The Chisholm correlation was confirmed to be the lowest accuracy among the correlations in the comparison. However a model coefficient of the Chisholm correlation used in Domanski and Hermes (2008) was for 90° bends and the viscous effect in the friction factor was neglected (see Sec. 3.4 and Appendix B). Padilla et al. (2009) and Padilla et al. (2012) also examined the applicability of the Chisholm correlation to two-phase flows of refrigerants. However they also used the model coefficient for 90° bends. Thus, in fact, the Chisholm correlation has not been sufficiently validated for U-bends yet.

Padilla et al. (2009) used available data of the bend pressure drop for three refrigerants, R-12, R410A and R-134a, in literature (Traviss and Rohsenow, 1973; Chen et al., 2004, 2007, 2008) to develop a bend pressure drop correlation. The database covers $3.25 \leq D \leq 8$ mm and $3.18 \leq D_B^* \leq 8.15$. They omitted the data of Geary in their database because of the different definition of the pressure drop in Geary's experiment. The bend pressure drop correlation proposed by Padilla et al. (2009) consists of the pressure drop for two-phase flows in straight pipes and the additional pressure drop due to bending of the flow. The former is given by an available pressure drop correlation for straight pipes (Muller-Steinhagen and Heck, 1986), and the latter is expressed in terms of the centrifugal forces acting on the two phases and its expression assures that this singular pressure drop vanishes when R_B becomes infinity. The proposed correlation gave better evaluations than the available correlations. Padilla et al. (2012) carried out experiments on the bend pressure drop of HFO-1234yf and R-134a refrigerants in horizontal U-bends of $D = 7.9$ and 10.85 mm and for $3.68 \leq D_B^* \leq 4.05$. The bend pressure drop was defined as the sum of the singular pressure drop in the bend and the additional pressure drops in the straight pipes caused by the presence of the bend. The Padilla correlation (Padilla et al., 2009) largely underestimated the bend pressure drops of these refrigerants.

As described above, the databases of the pressure drop in horizontal U-bends have been developed for refrigerants. In addition, most of the studies dealt with slug and annular flows

only (Domanski and Hermes, 2008; Padilla et al., 2012). Bend pressure drop data for typical flow patterns, i.e. bubbly, plug, slug and annular flows, in an air-water system would be of use in examining the applicability of the available correlations and in modeling the bend pressure drop.

In this study, pressure drop data for an air-water system were obtained for horizontally aligned U-bends to investigate characteristics of two-phase bend pressure drops for bubbly, plug, slug and annular flows, and to examine the applicability of the available correlations, i.e. Chen, Padilla, Domanski-Hermes and Chisholm correlations, to the data. The diameter D was 8 and 16 mm and D_B^* was 3 and 6. Although it is important to accurately make a channel geometry to obtain reliable pressure drop databases, it is not easy to make a bending pipe without any distortion and bends used in some previous studies have some distortion, e.g. de Oliveira and Barbosa (2014) and de Oliveira et al. (2014). We therefore made a bend section from two acrylic blocks machined to have half-circular cross section to obtain an accurate bend shape.

2. Experimental

2.1. Experimental setup

Figure 1 shows the experimental setup, which consists of the transparent U-bend placed in the horizontal plane, the two transparent straight pipes connected with the bend, the air-water mixing section, the water reservoir, the overflow tank, the pump (Iwaki, MD-70R) and the oil-free compressor (Hitachi, SRL-2). Air and water at room temperature (25±0.5 °C) and atmospheric pressure were used for the gas and liquid phases, respectively. The gas phase was supplied from the compressor to the mixing section through the regulator (TRUSCO, TP-3R21GB-8), the pressure gauge and the gas flowmeter (Nippon flow cell, FLT series). The liquid phase was supplied from the reservoir to the mixing section using the pump, and the volume flow rate was measured using the flowmeter (Nippon flow cell, SCO-4). The gas and liquid phases were mixed in the mixing section, and then, two-phase flows were formed and developed in the hydrodynamic entrance section. The two phases

flowed through the test section. Then the gas and liquid phases flowed out to atmosphere and to the overflow tank, respectively. The inner diameter, D, of the straight pipes was 8.0 and 16.1 mm. The ratio, D_B^*, of $2R_B$ to D was 3 and 6, where R_B is the bend radius of curvature (Fig. 2(a)). The bend was made of two acrylic blocks to assure the circular cross section and the constant bend radius of curvature (Fig. 2(b)). The length of the entrance section was larger than $130D$, with which the two-phase flows were confirmed to be fully developed at the inlet of the test section from the point of view of the pressure drop. The details will be given in Sec. 3.2.

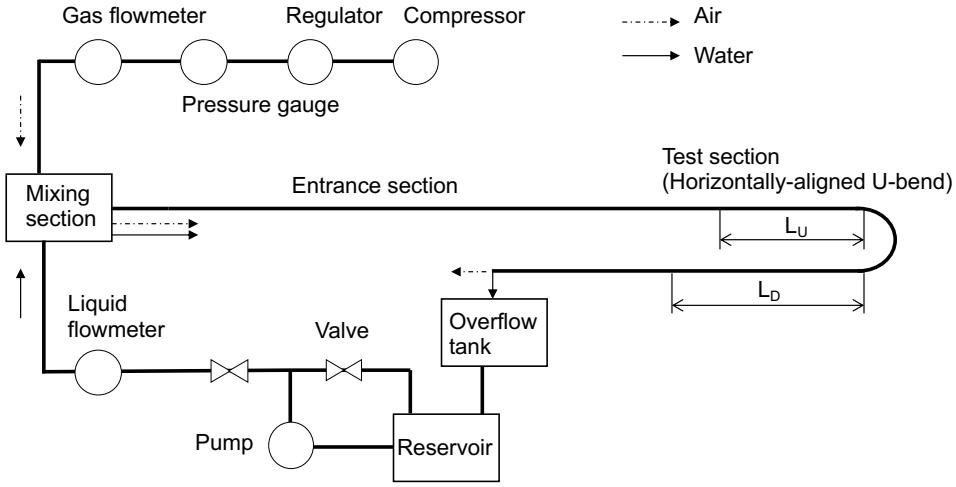

Figure 1: Experimental setup

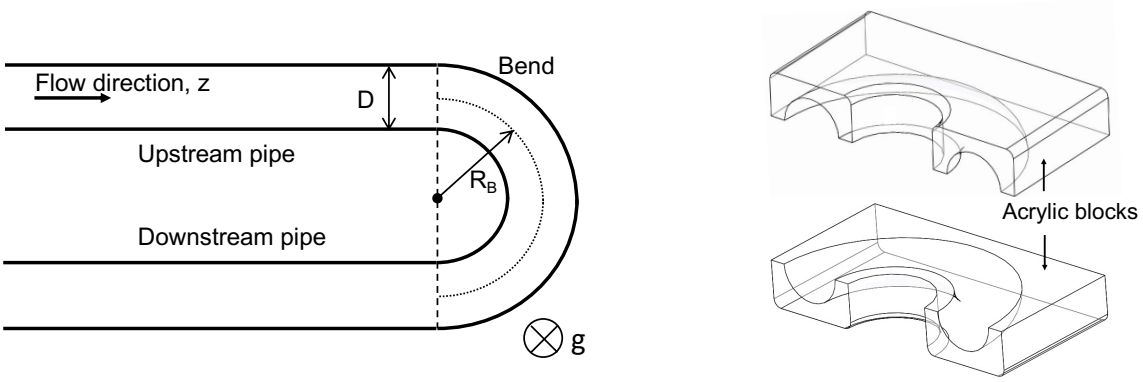

(a) U-bend (b) Bend part assembled with two blocks

Figure 2: U-bend configuration

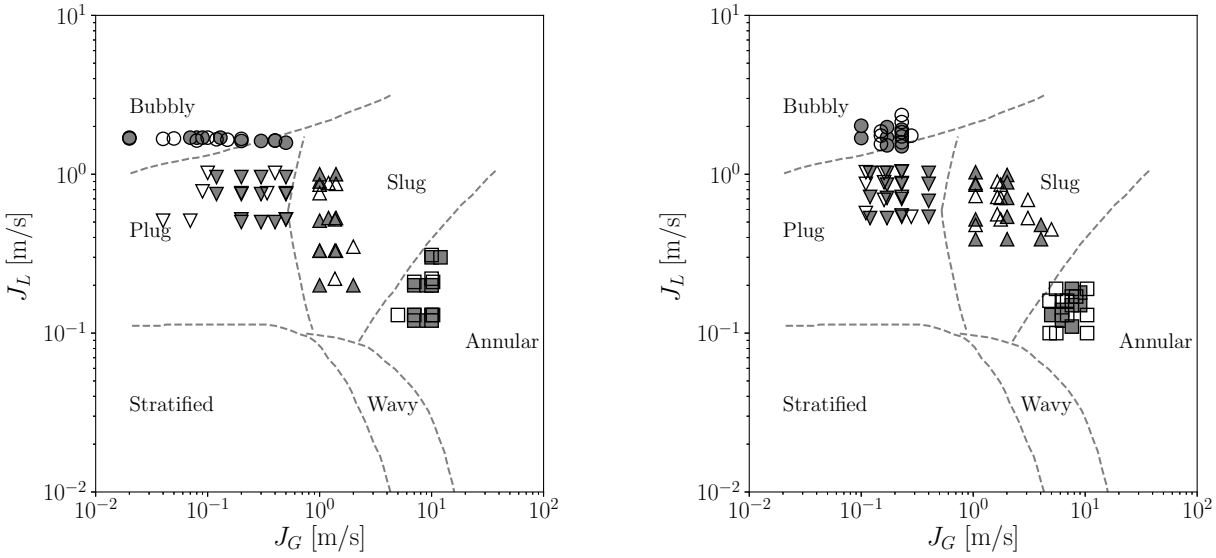

(a) $D = 16$ mm (b) $D = 8$ mm

Figure 3: Flow pattern maps in upstream straight pipes. Circle: bubbly flow, inversed-triangle: plug flow, triangle: slug flow, square: annular flow. Closed symbols: $D_B^* = 3$, open symbols: $D_B^* = 6$. The lines represent the flow pattern transition proposed by Barnea et al. (1980)

2.2. Experimental conditions and flow pattern map in upstream-side straight pipe

The gas and liquid volumetric fluxes, J_G and J_L, were varied so as to form various flow patterns, i.e. bubbly, plug, slug and annular flows. The ranges of J_G and J_L were $0.02 < J_G < 11$ m/s and $0.1 < J_L < 2.4$ m/s, respectively. Preliminary the gas and liquid volume flow rates were measured by downward displacement of water and by collecting water into a tank, respectively, to obtain reference values for calibration. The J_G and J_L evaluated with the flowmeters agreed with the reference values within $\pm 3\%$ and $\pm 1\%$ errors, respectively. Flows in the test section were observed using a high-speed video camera (IDT, MotionPro X-3). Figure 3 shows flow pattern maps in the upstream-side straight pipes identified from the high-speed video images. The present experimental condition covers the four flow patterns and the dependence of the flow pattern on J_G and J_L agrees with that in the flow pattern map developed by Barnea et al. (1980).

2.3. Measurement of bend pressure drop

The pressure drop, ΔP_B, caused by the presence of a bend can be divided into the following two parts, i.e. a pressure drop caused in the bend, $\Delta P_{B,U}$, and that in the straight pipe, $\Delta P_{B,P}$:

$$\Delta P_B = \Delta P_{B,U} + \Delta P_{B,P} \tag{1}$$

The two-phase bend pressure gradient is defined by

$$\left.\frac{\partial P}{\partial z}\right|_{B,TP} = \frac{\Delta P_B}{\pi R_B} \tag{2}$$

where z is the coordinate along the pipe axis. This definition is the same as that of Chisholm (Chisholm, 1980, 1983) and Padilla et al. (2009).

The pressure drop measurements were carried out using pressure difference transducers (Validyne, DP45 (accuracy: $\pm 0.5\%$ of full scale)). Pressure taps were mounted on the straight pipes as shown in Fig. 4. The sampling number and the sampling frequency were 60,000 and 1.0 kHz, respectively. The pressure transducer was calibrated for a static pressure of a liquid column in a vertical pipe. The measured static pressures were to within $\pm 1\%$ errors. The instantaneous pressure differences between two pressure taps were time-averaged. Fluctuation of the mean value decreased with increasing the sampling number and was confirmed to be within at least $\pm 2\%$ of the mean value by setting the sampling number to 60,000. Measurements of the friction coefficient in single-phase flows in the upstream-side straight pipe were also carried out to evaluate the measurement errors, confirming that the deviations from the Blasius correlation were to within $\pm 5\%$ for a wide range of the Reynolds number, i.e. from 3000 to $33,000$, which covers the experimental ranges of Re_L and Re_G, where Re_k is the Reynolds number of the phase k (see Sec. 3.4). Figure 5 shows an example of the pressure distributions in the pipe of $D = 8$ mm and $D_B^* = 6$. In the upstream of the bend, the pressure linearly decreases toward the bend as shown in the regression line. The bend effect on the pressure drop in the upstream pipe is therefore small. The presence of the bend causes a large pressure drop in the bend. The pressure gradient after passing through the bend approaches that in the upstream pipe (solid line), which means that the

flow disturbed in the bend is re-developing in the downstream pipe. Flows in far downstream of the bend outlet were confirmed to be fully-developed under all the conditions (see Sec. 3.2).

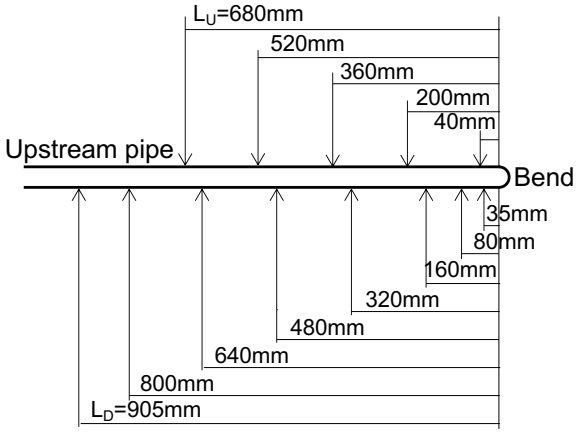

(a) $D = 16$ mm

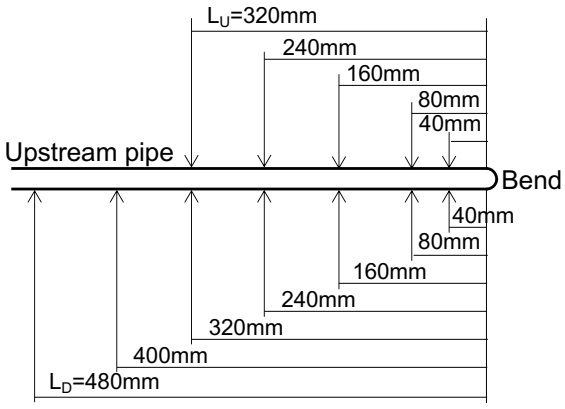

(b) $D = 8$ mm

Figure 4: Pressure tap location. The values represent the distance from the bend inlet (or outlet) to a tap location in the upstream pipe (or the downstream pipe).

A pressure drop, ΔP, between a pressure tap at L_U upstream from the bend entrance and that at L_D downstream from the bend outlet was measured, and then, ΔP_B was evaluated as $\Delta P_B = \Delta P - \partial P/\partial z|_{S,TP}\,(L_U + L_D)$, where $\partial P/\partial z|_{S,TP}$ is the two-phase pressure drop in the straight pipe. $L_U = 680$ mm and $L_D = 905$ mm for $D = 16$ mm and $L_U = 320$ mm and $L_D = 480$ mm for $D = 8$ mm.

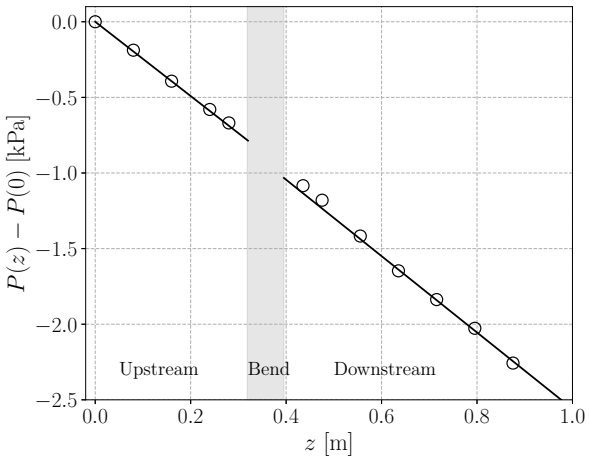

Figure 5: Pressure distribution along the pipe axis, where z is the axial coordinate and $P(0)$ is the pressure at 320 mm upstream from the bend entrance ($D = 8$ mm, $D_B^* = 6$, annular flow at (J_G, J_L) =(10.4 m/s, 0.13 m/s)).

3. Results and Discussion

3.1. Flows in U-bends

Figure 6(a) shows flows in the U-bend of $D = 16$ mm and $D_B^* = 3$. Note that the diameters of the straight pipe and the bend are the same, but they seem to be different in the images due to refraction at the pipe walls (The refraction is negligibly small in the bend section). In the bubbly flow, bubbles of various sizes are formed in the upstream pipe. The bend does not cause remarkable changes of the flow structure in the upstream pipe even just in front of the bend inlet, whereas the bend strongly affects the flow in it, i.e. bubbles immediately move to the inside of the bend (larger bend curvature side) after entering the bend due to the centrifugal force and they flow along the bend wall. The number of small bubbles seems to increase by passing the bend, implying that some bubble breakup takes place in the bend due to the increase in the velocity difference between the two phases. The maldistribution of the gas phase mitigates as bubbles flow toward downstream. The bubble size in the plug flow is much larger than in the bubbly flow because of the smaller J_L. The centrifugal force acting on the fluids in the bend causes the maldistribution of the phase fractions. Small bubbles flowing in the downstream straight pipe are generated

by bubble breakup. The image of the slug flow shows an instant of the passage of a large bubble through the bend. The liquid part in the bend outside (smaller bend curvature side) is much thicker than that in the bend inside due to the migration of the liquid toward the bend outside. The bend effect on the liquid film thickness can also be observed in the annular flow. In addition, the interface in the annular flow is largely disturbed at the bend outlet. Such disturbances in the interface sometimes grew into disturbance waves.

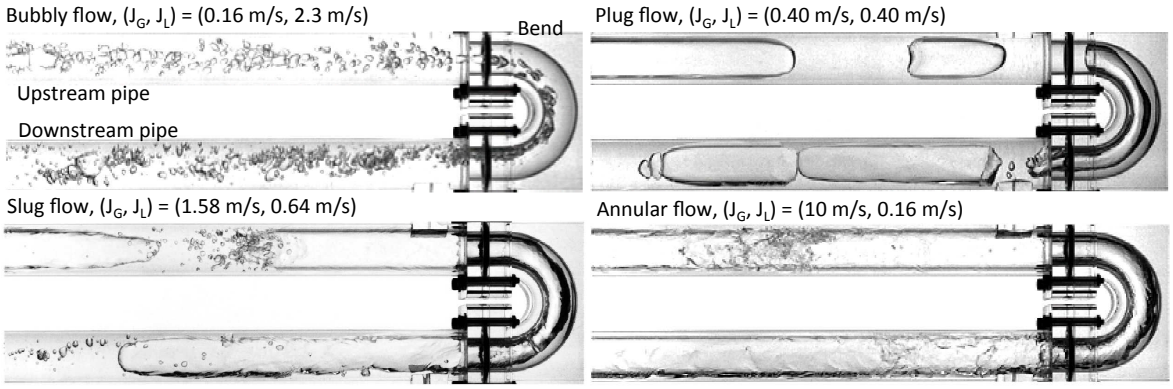

(a) $D = 16$ mm, $D_B^* = 3$

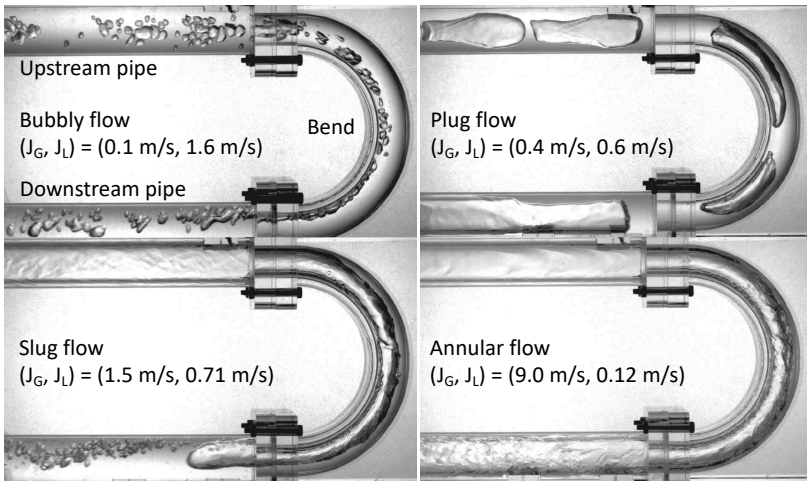

(b) $D = 16$ mm, $D_B^* = 6$

Figure 6: Flow patterns in U-bend of $D = 16$ mm (Bend part is made of two blocks to obtain accurate circular cross-section. The straight pipe and bend diameters are the same, but they seem different in the images due to refraction at the channel walls.)

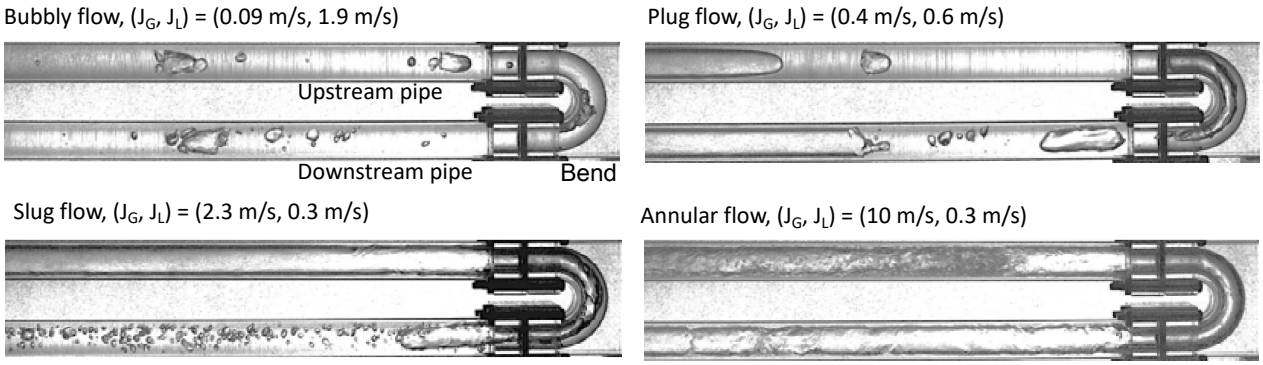

(a) $D = 8$ mm, $D_B^* = 3$

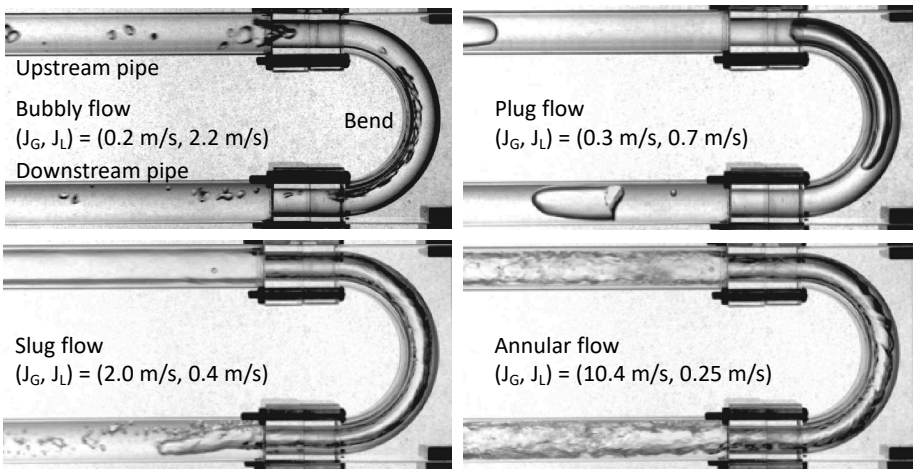

(b) $D = 8$ mm, $D_B^* = 6$

Figure 7: Flow patterns in U-bend of $D = 8$ mm

Figure 6(b) shows flows in the U-bend of $D = 16$ mm and $D_B^* = 6$. The two-phase centrifugal force F_c decreases by half with increasing D_B^* from 3 to 6 while keeping the inertial force F_i since F_c can be evaluated as $F_c = \rho_m J_T^2 D^3 / R_B = 2F_i / D_B^*$, where $F_i = \rho_m J_T^2 D^2$, J_T $(= J_L + J_G)$ is the total volumetric flux, and ρ_m the mixture density. In spite of the reduction in F_c, the bend effects, i.e. the accumulation of the gas phase toward the bend inside and the maldistribution of the phases in the downstream pipe, are still present. Two-phase flows in the smaller pipe ($D = 8$ mm) with $D_B^* = 3$ and 6 are shown in Figs. 7(a) and (b), respectively. The bend effects are similar to those in the flows for $D = 16$ mm.

3.2. Two-Phase Multipliers in Upstream and Downstream Straight Pipes

The two-phase multiplier, ϕ_{L0}, in the upstream straight pipe is compared with available correlations (Beattie and Whalley, 1982; Muller-Steinhagen and Heck, 1986) to confirm that the flows were fully-developed before entering the bends, where the subscript $L0$ denotes that the variable is for the flow assumed to be single-phase liquid. Beattie and Whalley (1982) proposed the mixture viscosity $\mu = \mu_L(1 + 2.5\beta) + \mu_G\beta$, and with this viscosity ϕ_{L0} is given by

$$\phi_{L0}^2 = \left[1 + x\left(\frac{\rho_L}{\rho_G} - 1\right)\right]\left[(1-\beta)(1+2.5\beta) + \frac{\mu_G}{\mu_L}\beta\right]^{0.25} \tag{3}$$

where β is the ratio of the volume flow rates defined by

$$\beta = \frac{J_G}{J_G + J_L} \tag{4}$$

Muller-Steinhagen and Heck (1986) proposed the following pressure drop correlation:

$$\left.\frac{\partial P}{\partial z}\right|_{S,TP} = \left[\left.\frac{\partial P}{\partial z}\right|_{S,L0} + 2x\left(\left.\frac{\partial P}{\partial z}\right|_{S,G0} - \left.\frac{\partial P}{\partial z}\right|_{S,L0}\right)\right](1-x)^{1/3} + \left.\frac{\partial P}{\partial z}\right|_{S,G0} x^3 \tag{5}$$

where x is the quality and $\partial P/\partial z|_{S,k0}$ the single-phase pressure drop of phase k given by

$$\left.\frac{\partial P}{\partial z}\right|_{S,k0} = \frac{\lambda_{k0} G^2}{2D\rho_k} \tag{6}$$

where G is the mass flux. The friction factor λ_{k0} and the Reynolds number in this correlation are defined as

$$\lambda_{k0} = \begin{cases} \dfrac{64}{Re_{k0}} & \text{for } Re_{k0} < 1187 \\ \dfrac{0.3164}{Re_{k0}^{0.25}} & \text{otherwise} \end{cases} \tag{7}$$

$$Re_{k0} = \frac{GD}{\mu_k} \tag{8}$$

The present data are compared with the correlations in Fig. 8. Good agreements confirm the fully-developed state of the two-phase flows in the upstream pipe for all the flow patterns.

Figure 9 shows comparisons between the two-phase multipliers in upstream of the bend inlet and in far downstream the bend outlet. They agree with each other under all the conditions. Hence the flows re-developed in far downstream from the bend outlet from the point of view of the pressure gradient.

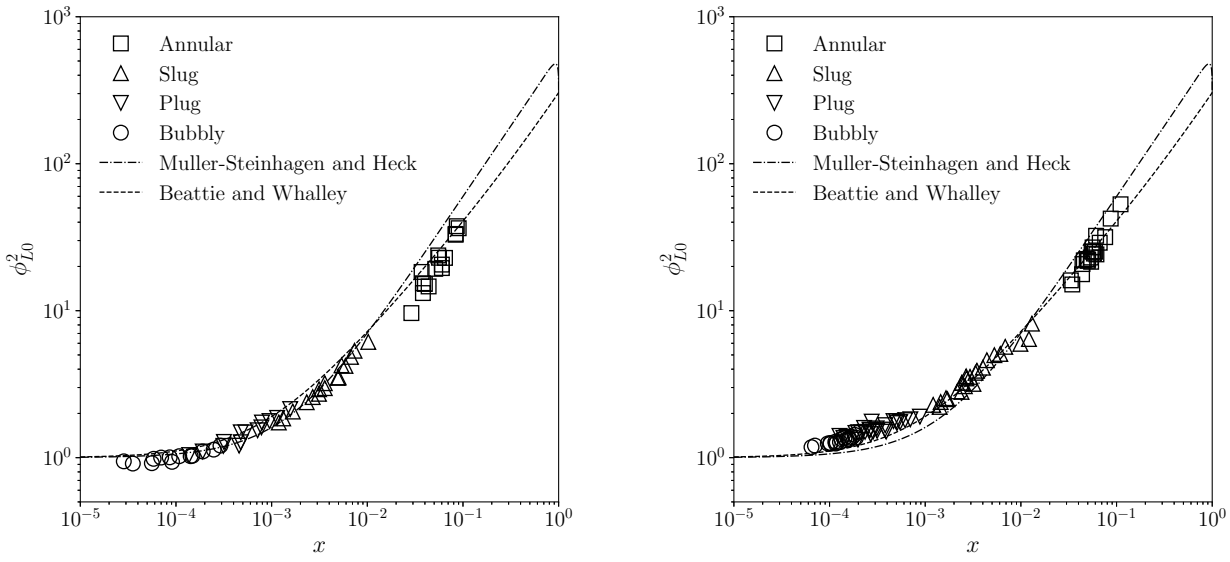

(a) $D = 16$ mm

(b) $D = 8$ mm

Figure 8: Comparisons between two-phase multipliers in upstream straight pipe and available correlations

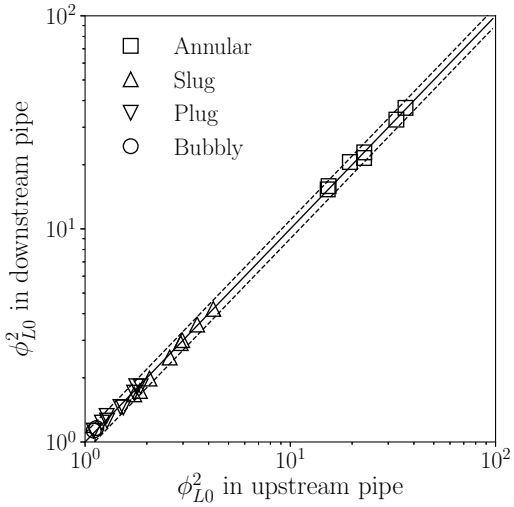

(a) $D = 16$ mm, $D_B^* = 3$

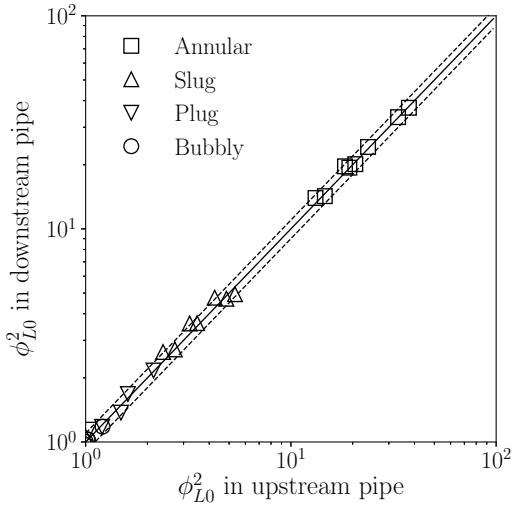

(b) $D = 16$ mm, $D_B^* = 6$

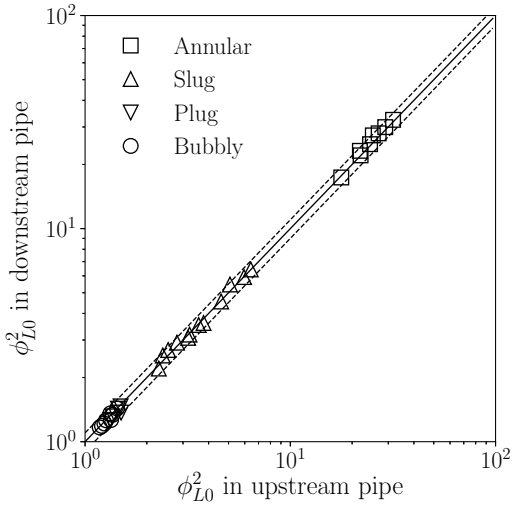

(c) $D = 8$ mm, $D_B^* = 3$

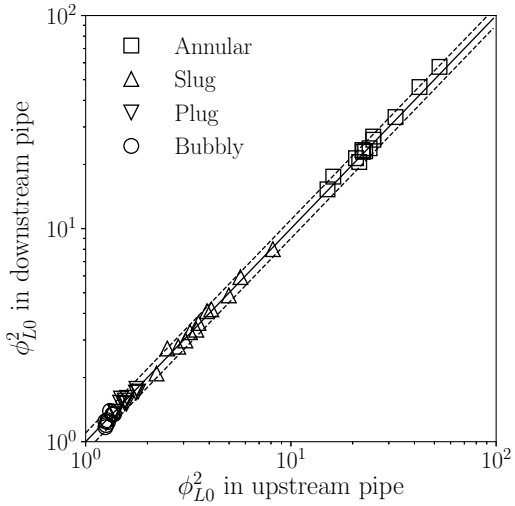

(d) $D = 8$ mm, $D_B^* = 6$

Figure 9: Comparisons between two-phase multipliers in upstream and downstream straight pipes. The solid line represents 0% difference, and the dashed line show 10% errors.

3.3. ΔP_B in each Flow Pattern

Figure 10(a) shows ΔP_B for $D = 16$ mm and $D_B^* = 3$. The sizes of the circles represent the magnitude of ΔP_B and the reference size for $100Pa$ is shown in the figure legend. In the plug flow regime, the increase in J_L increases ΔP_B and its effect is much larger than that of J_G in the present experimental range. The ΔP_B in the bubbly flow regime are larger than those in the plug flow regime because of larger J_L, and the effect of J_G on ΔP_B is not visible even with the wide range of J_L, i.e. J_L from 0.01 to 0.5 m/s. The effects of J_L and J_G in the slug flow regime are similar to those in the plug flow regime. The ΔP_B in the slug flow regime is larger than that in the plug flow regime for the same J_L. In the annular flow regime, the increase in both J_L and J_G increases ΔP_B. The ΔP_B of the annular flows at $J_L = 0.3$ m/s are comparable to those in the bubbly flow regime of $J_L \sim 1.6$ m/s. Comparing Fig. 10(a) and (b) for $D = 16$ mm and $D_B^* = 6$ confirms that the orders of ΔP_B at the same J_L and J_G are similar, meaning that the effects of D_B^* on ΔP_B are much smaller than those of the superficial velocities.

The ΔP_B for $D = 8$ mm are shown in Fig. 10(c) and (d). The trends of ΔP_B for the superficial velocities in each phase are the same as those of $D = 16$ mm. Further analyses of the characteristics of the pressure drop will be carried out in the form of the two-phase multiplier in the following sections.

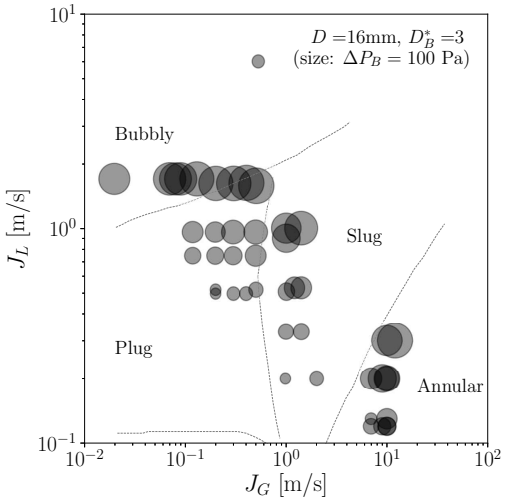

(a) $D = 16$ mm, $D_B^* = 3$

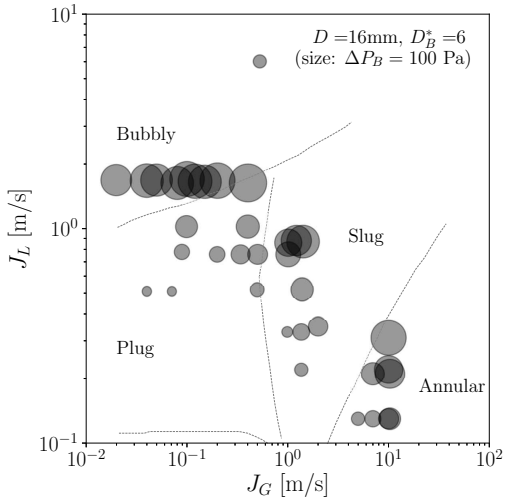

(b) $D = 16$ mm, $D_B^* = 6$

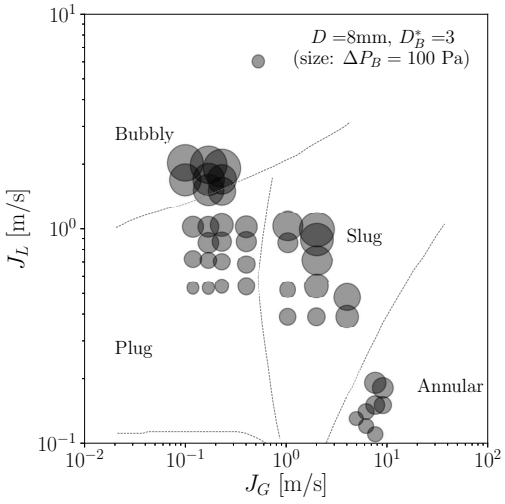

(c) $D = 8$ mm, $D_B^* = 3$

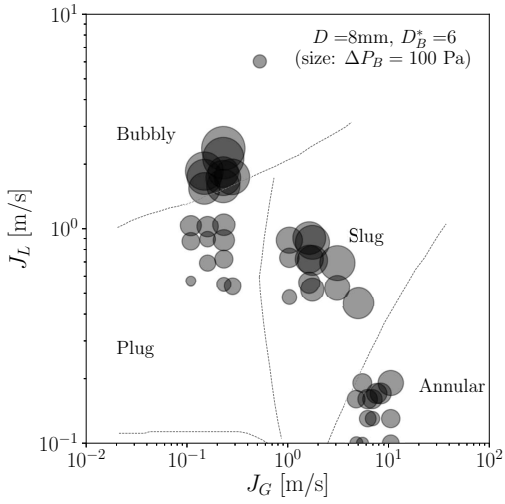

(d) $D = 8$ mm, $D_B^* = 6$

Figure 10: Bend pressure drops, ΔP_B. The circle radius is proportional to the magnitude of ΔP_B and the reference size for 100 Pa is shown in each figure. The lines represent the flow pattern transition in Barnea et al. (1980).

3.4. Comparisons between pressure drop data and available correlations

Available correlations of the bend pressure gradient are compared with the present air-water data in this section. The correlations tested are those proposed in Chen et al. (2004), Domanski and Hermes (2008), Padilla et al. (2009) and Chisholm (1983). It should be noted that the first three correlations were developed for refrigerants, and therefore, the present experimental range is outside of their applicable ranges. Comparisons with pressure drop data of refrigerants can be found in their papers. See Appendix A for their experimental conditions.

Chen et al. (2004) proposed the following bend pressure drop correlation by introducing the liquid viscosity and surface tension effects into the Geary correlation:

$$\left.\frac{\partial P}{\partial z}\right|_{B,TP} = \lambda_{B,TP}\frac{\rho_G J_G^2}{2D} \tag{9}$$

where the two-phase bend friction coefficient, $\lambda_{B,TP}$, is given by

$$\lambda_{B,TP} = \frac{0.01 Re_m^{0.35}}{We_{G0}^{0.12} x^{1.26}\exp(0.194 D_B^*)} \tag{10}$$

where Re_m and We_{G0} are the total Reynolds number and the gas Weber number, respectively, defined by

$$Re_m = Re_G + Re_L \tag{11}$$

$$We_{G0} = \frac{G^2 D}{\rho_G \sigma} \tag{12}$$

The Reynolds number of the phase k ($= G$ or L) is defined by

$$Re_k = \frac{\rho_k J_k D}{\mu_k} \tag{13}$$

The Domanski-Hermes correlation is given by

$$\left.\frac{\partial P}{\partial z}\right|_{B,TP} = \Lambda_B \left.\frac{\partial P}{\partial z}\right|_{S,TP} \tag{14}$$

where $\partial P/\partial z|_{S,TP}$ is given by making use of an available correlation for straight pipes (Muller-Steinhagen and Heck, 1986). The bend effect multiplier Λ_B is given by

$$\Lambda_B = 6.5\times 10^{-3} Re_G^{0.54} D_B^{*-0.67}\left(\frac{1}{x}-1\right)^{0.21}\left(\frac{\rho_L}{\rho_G}\right)^{0.34} \tag{15}$$

Padilla et al. (2009) correlated $\partial P/\partial z|_{B,TP}$ in terms of the frictional and singular pressure drops, i.e.

$$\left.\frac{\partial P}{\partial z}\right|_{B,TP} = \left.\frac{\partial P}{\partial z}\right|_{S,TP} + \left.\frac{\partial P}{\partial z}\right|_{\mathrm{sing},TP} \tag{16}$$

The former is given by the Muller-Steinhagen-Heck correlation (Muller-Steinhagen and Heck, 1986) and the latter is given by

$$\left.\frac{\partial P}{\partial z}\right|_{\mathrm{sing},TP} = 0.047 \left(\frac{\rho_G J_G^2}{R_B}\right) \left(\frac{J_L^2}{R_B}\right)^{1/3} \tag{17}$$

Chisholm (1980) applied the Lockhart-Martinelli correlation to two-phase flows in 90° bends and confirmed that the pressure drop data obtained by Sekoguchi et al. (1969) were well evaluated using the correlation. Chisholm also extended his correlation for U-bends as

$$\left.\frac{\partial P}{\partial z}\right|_{B,TP} = \phi_{B,L}^2 \left.\frac{\partial P}{\partial z}\right|_{B,L} \tag{18}$$

where $\partial P/\partial z|_{B,L}$ is the liquid-phase pressure gradient in the bend, and $\phi_{B,L}$ the bend two-phase multiplier, which is given by a function of the Lockhart-Martinelli parameter, X_B, for a bend defined by (Sekoguchi et al., 1969)

$$X_B^2 = \frac{\left.\frac{\partial P}{\partial z}\right|_{B,L}}{\left.\frac{\partial P}{\partial z}\right|_{B,G}} \tag{19}$$

where $\partial P/\partial z|_{B,G}$ is the gas-phase pressure gradient in the bend. We evaluated the single-phase pressure gradients using the following correlation proposed by Idelchik (1986):

$$\left.\frac{\partial P}{\partial z}\right|_{B,k} = \xi_{B,k} \frac{\rho_k J_k^2}{2\pi R_B} \tag{20}$$

where $\xi_{B,k}$ is the bend friction coefficient given by

$$\xi_{B,k} = 0.294 \left(\frac{2}{D_B^*}\right)^m + \frac{\pi D_B^*}{2} \lambda_k \tag{21}$$

where $m = 2.5$ for $1 \leq D_B^* \leq 2$ and $m = 1/2$ for $D_B^* > 2$, and λ_k is the single-phase friction factor for straight pipes given by

$$\lambda_k = \frac{0.3164}{Re_k^{1/4}} \tag{22}$$

The $\xi_{B,L}$ of water was measured in the present experiment to examine the validity of Eq. (21), and the results confirmed that Idelchik's correlation can give reasonable evaluations of the single-phase bend pressure drops in the present experimental range. By using Eq. (20), X_B can be written as

$$X_B^2 = \frac{\xi_{B,L}\rho_L J_L^2}{\xi_{B,G}\rho_G J_G^2} \tag{23}$$

Chisholm (1983) proposed the following correlation for $\phi_{B,L}$:

$$\phi_{B,L}^2 = 1 + \frac{C_B}{X_B} + \frac{1}{X_B^2} \tag{24}$$

where the parameter C_B is given by

$$C_B = \frac{B(\Gamma_B^2 - 1) + 2^{2-n} - 2}{\Gamma_B} \tag{25}$$

When $1/\Gamma_B^2 \ll 1$, C_B can be approximated as

$$C_B = \Gamma_B B \tag{26}$$

Here B is a coefficient accounting for a change in the relative velocity between the two phases due to the bend and Γ_B is the physical property index defined by

$$\Gamma_B^2 = \left(\frac{\rho_L}{\rho_G}\right)\left(\frac{\mu_G}{\mu_L}\right)^n \tag{27}$$

The model coefficient n in Eq. (27) is the power of the Reynolds number in the expression of $\xi_{B,L0}$ in the form of $\xi_{B,L0} = A/Re_{L0}^n$, where A is a constant. The n was evaluated by fitting this functional form to the single-phase bend pressure drop model (Idelchik, 1986). The n and A are shown in Table 1.

The coefficient B is given by

$$B = \frac{1}{2}(1 + B_{90}) \tag{28}$$

where B_{90} is the coefficient for 90° bends:

$$B_{90} = 1 + \frac{4.4}{\xi_{B,L0}(4 + D_B^*)} \tag{29}$$

The B for U-bends are smaller than B_{90}; for example, $B/B_{90} = 0.69$ when $D_B^* = 3$ and $\xi_{B,L0} = 0.4$, which is a typical value in the present experiments. In comparisons between the

Table 1: Coefficients in $\xi_{B,L0} = A/Re_{L0}^n$

D_B^*	3	6
n	0.094	0.158
A	0.93	2.0

Chisholm correlation and $\partial P/\partial z|_{B,TP}$ reported in Domanski and Hermes (2008) and Padilla et al. (Padilla et al., 2009, 2012), B_{90} was used though the bend angle in their experimental databases were 180°. Mandal and Das (2001) applied the correction for the bend angle, Eq. (28), when comparing the Chisholm correlation with their experimental data, whereas B_{90} was incorrectly given as $B_{90} = 4.4/\xi_{B,L0}(4 + D_B^*)$. It should also be noted that they used the Chisholm correlation in the so-called B-coefficient form (Chisholm, 1983; Azzi et al., 2000):

$$\phi_{B,L0}^2 = 1 + \left(\frac{\rho_L}{\rho_G} - 1\right)\left(Bx(1-x) + x^2\right) \tag{30}$$

This form does not account for the effects of the viscosity ratio represented by the power n in $\xi_{B,L0}$, although Chisholm (1980, 1983) proposed the following more general form:

$$\phi_{B,L0}^2 = 1 + (\Gamma_B^2 - 1)\left(Bx^{(2-n)/2}(1-x)^{(2-n)/2} + x^{2-n}\right) \tag{31}$$

It can be shown that the B-coefficient form is identical with the C-coefficient form, Eq. (24), provided that $n = 0$. Even when $n \neq 0$, the C-coefficient form is approximately the same as the B-coefficient form, i.e., solving Eq. (24) for $\phi_{B,L0}^2$ and neglecting the following factor in the resultant equation of $\phi_{B,L0}^2$ yield Eq. (31):

$$D_R = (1-x)^{2-n} + (2^{2-n} - 2)x^{(2-n)/2}(1-x)^{(2-n)/2} + x^{2-n} - 1 \tag{32}$$

This term is usually negligible since it is not more than 0.025 for $n = 0.25$ (Chisholm, 1983).

Figure 11 shows comparisons between $\partial P/\partial z|_{B,TP}$ calculated using the correlations and the present air-water data, and the mean absolute error, MRE, the mean relative error,

MAE, and the percentage of data points within ±30% error band are tabulated in Table 2, where MRE and MAE are defined by

$$\mathrm{MRE} = \frac{1}{N}\sum_{i=1}^{N}\left(\frac{X_i^c - X_i^m}{X_i^m}\right) \tag{33}$$

$$\mathrm{MAE} = \frac{1}{N}\sum_{i=1}^{N}\left|\frac{X_i^c - X_i^m}{X_i^m}\right| \tag{34}$$

where X is a measured item ($\partial P/\partial z|_{B,TP}$), the superscripts c and m represent its calculated and measured values, respectively, and N is the total number of the data points ($N = 166$ in the present study). The Chen correlation gives good evaluations only for slug and annular flows, and the errors in the other flow patterns are large. The Domanski-Hermes correlation is more accurate except for the annular flow data. However the large errors in the annular flow data make MRE and MAE much larger than Chen's correlation. The evaluations obtained using the Padilla correlation are reasonable only for annular flows and the correlation tends to underestimate the pressure gradient as shown by the large negative value of MRE. Among the correlations examined, the Chisholm correlation is the most accurate from the point of view of MAE, where the C-coefficient form, Eq. (24), is used. This correlation however tends to overestimate the pressure drop in annular flows, and the errors in the annular flow regime are relatively larger than in the other flow regimes. This makes MRE comparable to MAE. Errors evaluated for the B-coefficient form, Eq. (31), are also given in the table (figures are given in Appendix B). Being similar to the C-coefficient form, the B-coefficient form gives much better evaluations than the other correlations whereas the errors tend to be large in the annular flow regime.

Table 2: Evaluations of errors in calculated $\partial P/\partial z|_{B,TP}$

	MRE [%]	MAE [%]	±30 error band [%]
Chen et al. (2004)	−15.8	36.5	46.4
Domanski and Hermes (2008)	41.6	68.3	44.0
Padilla et al. (2009)	−53.3	54.8	15.7
Chisholm (1983) (C-form, Eq. (24))	24.7	30.4	63.9
Chisholm (1983) (B-form, Eq. (31))	11.8	27.3	71.1
Proposed (Eq. (37))	6.8	21.8	74.7
Proposed (Eq. (38))	−2.8	17.8	85.5

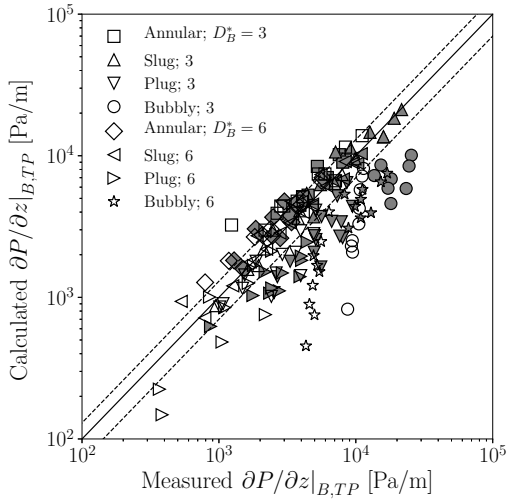

(a) Chen correlation

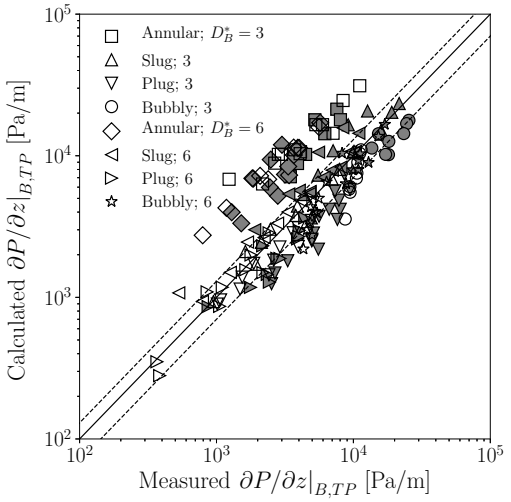

(b) Domanski-Hermes correlation

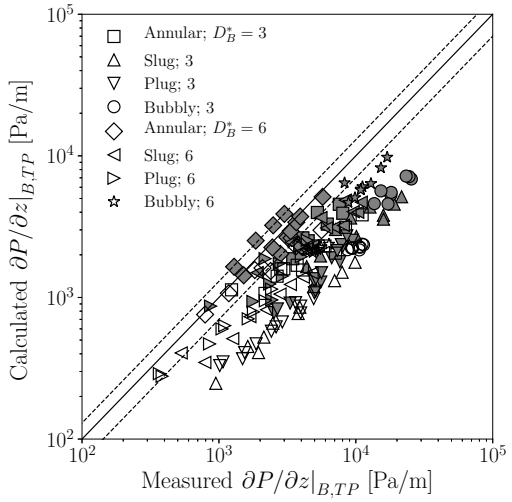

(c) Padilla correlation

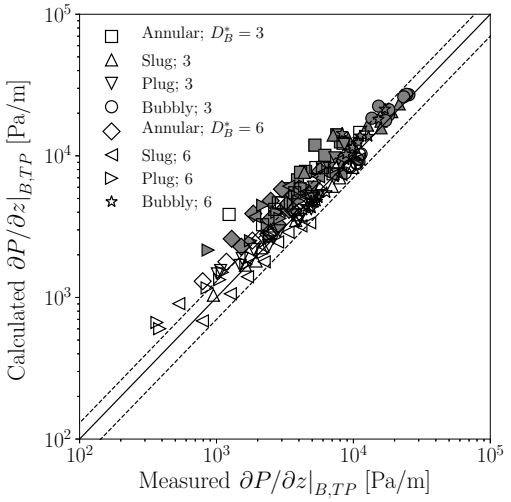

(d) Chisholm correlation, Eq. (24)

Figure 11: Comparisons between bend pressure gradients calculated using available correlations and air-water data. Open symbols: $D = 16$ mm, closed symbols: $D = 8$ mm. The dashed lines represent $\pm 30\%$ errors.

3.5. Chisholm-type correlation for present data

Figure 13 shows $\phi_{B,L}$ plotted against X_B. The $\phi_{B,L}$ for all the flow patterns are well correlated in terms of X_B. However, as discussed in the previous section, the Chisholm correlation represented by the dashed line overestimates the bend pressure gradients in annular flows, where $C_B = 37$ was used to draw the correlation line, although the correlation agrees well with the data of the bubbly, plug and slug flows. The Chisholm-type correlation is therefore separately fitted to the data of annular flow and the other flow pattens as follows:

$$\phi^2_{B,L;a} = \left(\frac{C_B}{2X_B}\right)^{0.83} + \frac{10}{X_B^{1.6}} \quad \text{for annular flows} \tag{35}$$

$$\phi^2_{B,L;o} = 1 + \left(\frac{C_B}{X_B}\right)^{0.83} \quad \text{for the other flow patterns} \tag{36}$$

Combining these expressions yields

$$\phi_{B,L} = \max[\phi_{B,L;a}, \phi_{B,L;o}] \tag{37}$$

This equation gives good evaluations of $\phi_{B,L}$ and $\partial P/\partial z|_{B,TP}$ as shown in Figs. 12 (solid line) and 13, respectively. In fact, the original B-coefficient form is slightly better than the correlation, $\phi_{B,L;o}$, for bubbly, plug and slug flows. Hence one can use $\phi_{B,L;a}$ for the annular flow regime and the B-coefficient form for the others, i.e.

$$\begin{cases} \phi^2_{B,L} = \phi^2_{B,L;a} & \text{for annular flows} \\ \phi^2_{B,L0} = 1 + (\Gamma_B^2 - 1)\left(Bx^{(2-n)/2}(1-x)^{(2-n)/2} + x^{2-n}\right) & \text{for the other flow patterns} \end{cases} \tag{38}$$

This combination gives the best result among the correlations examined as shown in Fig. 14 and Table 2. The applicability of the Lockhart-Martinelli method for U-bends and the empirical correlation to two-phase flows of different fluid properties will be examined in our future study.

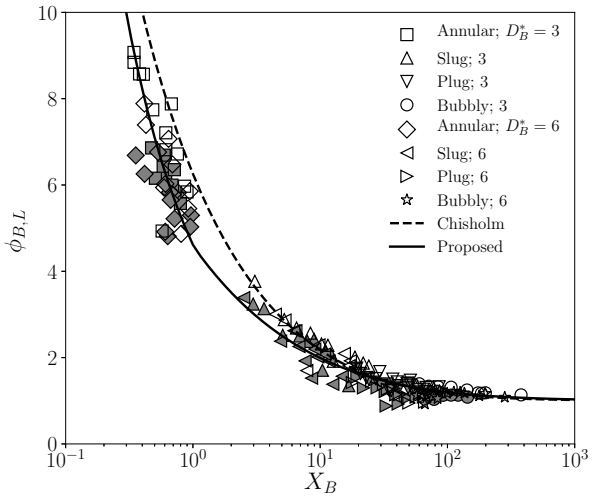

Figure 12: Bend pressure drop multiplier plotted against modified Lockhart-Martinelli parameter. Open symbols: $D = 16$ mm, closed symbols: $D = 8$ mm. The data are comparison with Eq. (24) and (37) (Broken-line: Eq. (24)), Solid line: Eq. (37)

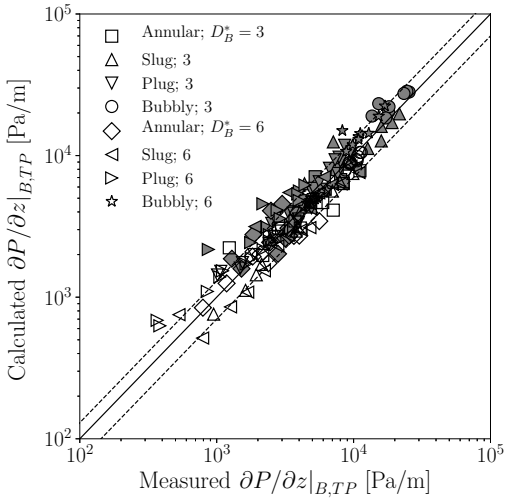

Figure 13: Comparisons between bend pressure gradients calculated using Eq. (37) and air-water data. Open symbols: $D = 16$ mm, closed symbols: $D = 8$ mm.

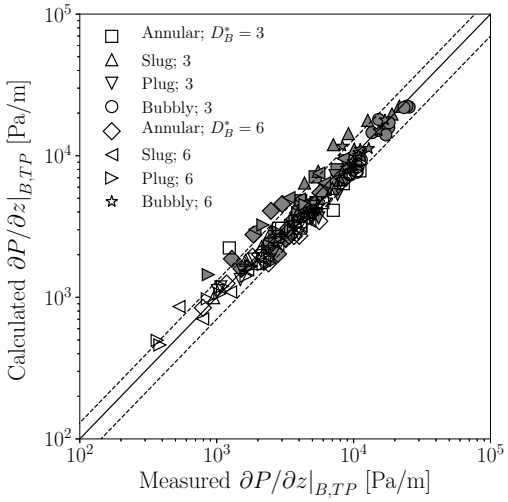

Figure 14: Comparisons between bend pressure gradients calculated using Eq. (38) and air-water data. Open symbols: $D = 16$ mm, closed symbols: $D = 8$ mm.

4. Conclusion

The pressure drops in horizontally aligned U-bends were measured for air-water bubbly, plug, slug and annular flows to examine the validity of available bend pressure drop correlations. The inner diameters, D, of the U-bends were 8 and 16 mm, and the bend ratios, $D_B^* = 2R_B/D$, were 3 and 6, where R_B is the bend radius of curvature. Since the presence of the bend disturbed the flow and induced large pressure drops not only within the bend but also in the downstream-side straight pipe, the bend pressure drop was evaluated as the sum of the pressure drop caused within the bend and the extra pressure drop caused in the re-developing region in the downstream-side straight pipe. The ranges of the gas and liquid volumetric fluxes, J_G and J_L, were $0.02 < J_G < 11$ m/s and $0.1 < J_L < 2.4$ m/s, respectively, to cover the above-mentioned flow patterns. As a result, the following conclusions were obtained:

1. The bend two-phase multiplier is well correlated in terms of the modified Lockhart-Martinelli parameter.

2. The Chisholm correlation gives better evaluations of the bend pressure gradients than other available correlations, i.e. the Chen, Domanski-Hermes and Padilla correlations, though the errors in annular flows are relatively larger than those in the other flow patterns.

3. The present data of the bend two-phase multiplier are expressed well by using an empirical correlation making use of the fundamental functional form of the Chisholm correlation.

Acknowledgement

The authors would like to express their sincere thanks to Mr. Daiki Suzuki and Mr. Tomoki Kitayama for their support in experiments.

Appendix A. Bend Pressure Drop Correlations

The bend pressure drop correlations proposed by Chen et al. (2004), Domanski and Hermes (2008), Padilla et al. (2009) and Chisholm (1983) are tabulated in Table A.1. The first three correlations were developed by using pressure drop databases of refrigerants in U-bends as shown in Table A.2. Though the present experimental condition of $D = 8$ mm and $D_B^* = 6$ is within the geometrical conditions of Chen et al. (2004), Domanski and Hermes (2008) and Padilla et al. (2009), the bend size of $D = 16$ mm is larger and $D_B^* = 3$ is smaller than in their experiments. Experimental data of pressure drops in air-water two-phase flows in 90° bends obtained by Sekoguchi et al. (1969) were used to examine the validity of the Chisholm correlation (Chisholm, 1980).

Appendix B. Evaluation of Bend Pressure Gradient Using B-Coefficient Form of Chisholm Correlation

The B-coefficient form, Eq. (30), of the Chisholm correlation used in the literature (Azzi et al., 2000; Mandal and Das, 2001; Domanski and Hermes, 2008; Padilla et al., 2009; Tay and Thorpe, 2014) is examined. Figure B.1(a) shows bend pressure gradients calculated using

Table A.1: Available pressure gradient corrleations. C2004:Chen et al. (2004), DH2012:Domanski and Hermes (2008), P2009:Padilla et al. (2009), C1983:Chisholm (1983)

	Pressure gradient	Multiplier	
C2004	$\frac{\partial P}{\partial z}\big\vert_{B,TP} = \lambda_{B,TP}\frac{\rho_G J_G^2}{2D}$	$\lambda_{B,TP} = \frac{0.01 Re_m^{0.35}}{We_{G0}^{0.12} x^{1.26}\exp(0.194 D_B^*)}$	$Re_m = Re_G + Re_L$ $We_{G0} = G^2 D/\rho_G\sigma$ $Re_k = \rho_k J_k D/\mu_k$
DH2012	$\frac{\partial P}{\partial z}\big\vert_{B,TP} = \Lambda_B \frac{\partial P}{\partial z}\big\vert_{S,TP}$	$\Lambda_B = 6.5\times10^{-3} Re_G^{0.54} D_B^{*-0.67}\left(\frac{1}{x}-1\right)^{0.21}\left(\frac{\rho_L}{\rho_G}\right)^{0.34}$	
P2009	$\frac{\partial P}{\partial z}\big\vert_{B,TP} = \frac{\partial P}{\partial z}\big\vert_{S,TP} + \frac{\partial P}{\partial z}\big\vert_{\mathrm{sing},TP}$	$\frac{\partial P}{\partial z}\big\vert_{\mathrm{sing},TP} = a\left(\frac{\rho_G J_G^2}{R_B}\right)\left(\frac{J_L^2}{R_B}\right)^b$	$a = 0.047\ \mathrm{s}^{2/3}/\mathrm{m}^{1/3}$ $b = 1/3$
C1983	(C-form) $\frac{\partial P}{\partial z}\big\vert_{B,TP} = \phi_{B,L}^2 \frac{\partial P}{\partial z}\big\vert_{B,L}$	$\phi_{B,L}^2 = 1 + \frac{C_B}{X_B} + \frac{1}{X_B^2}$	$X_B^2 = \frac{\xi_{B,L}\rho_L J_L^2}{\xi_{B,G}\rho_G J_G^2}$ $C_B = \Gamma_B B$ $B = (1+B_{90})/2$ $B_{90} = 1 + \frac{4.4}{\xi_{B,L0}(4+D_B^*)}$ $\Gamma_B^2 = (\rho_L/\rho_G)(\mu_G/\mu_L)^n$
	(B-form) $\frac{\partial P}{\partial z}\big\vert_{B,TP} = \phi_{B,L0}^2 \frac{\partial P}{\partial z}\big\vert_{B,L0}$	$\phi_{B,L0}^2 = 1 + (\Gamma_B^2 - 1)\left(Bx^{(2-n)/2}(1-x)^{(2-n)/2} + x^{2-n}\right)$	

Eq. (30). Being similar to the C-coefficient form, the B-coefficient form gives reasonable evaluations except for the annular flow regime. However MAE with the B-form (41.5%) is larger than the C-form (30.4%). The reason of this difference can be understood by testing the B-coefficient form with $n \neq 0$, Eq. (31), as shown in Fig. B.1(b). Accounting for the effects of the viscosity ratio remarkably improves the accuracy. Its MAE of 27.3% is similar to that with the C-coefficient form. This result confirms that the C-coefficient and B-coefficient forms are almost the same as described in Sec. 3.4.

Table A.2: Fluid and bend geometries considered in model developments. C2004:Chen et al. (2004), DH2012:Domanski and Hermes (2008), P2009:Padilla et al. (2009), C1983:Chisholm (1983)

	Fluid	D_B [mm]	D_B^*	data source
C2004	R-410A	3.3−11.6	3.9−8.15	Geary (1975); Wang et al. (2003), Experiment
DH2012	R-22, R-410A	3.3−11.6	3.9−8.15	Geary (1975); Chen et al. (2004)
P2009	R-12, R-134a, R-410A	3.25−8.0	3.18−8.15	Traviss and Rohsenow (1973); Chen et al. (2004); Chen et al. (2007, 2008)
C1983	air-water	18, 25.7	4.72, 10.0	Sekoguchi et al. (1969) (90° bends)
Present	air-water	8, 16	3, 6	Experiment

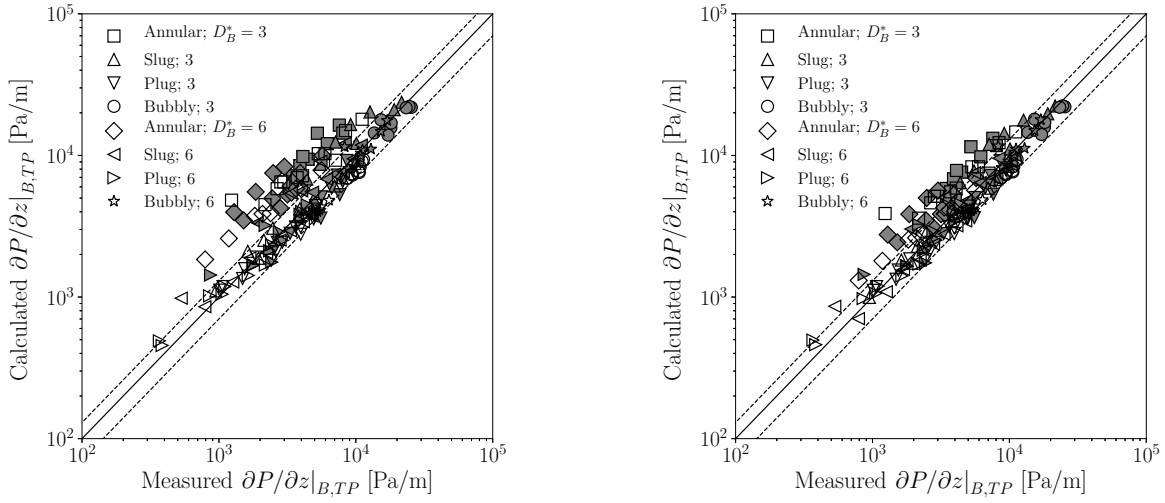

(a) B-coefficient form with $n = 0$ (Eq. (30)) (b) B-coefficient form with $n \neq 0$ (Eq. (31))

Figure B.1: Evaluations of bend pressure gradients by using the Chisholm correlation in the B-coefficient form. Open symbols: $D = 16$ mm, closed symbols: $D = 8$ mm. The dashed lines represent ±30% errors.

References

Azzi, A., Belaadi, S., Friedel, L., 2000. Two-phase gas/liquid flow pressure loss in bends. Forschung im Ingenieurwesen 65(10), 309–318.

Barnea, D., Shoham, O., Taitel, Y., 1980. Flow pattern transition for gas-liquid flow in horizontal and inclined pipes. International Journal of Multiphase Flow 6, 217–225.

Beattie, D. R. H., Whalley, P. B., 1982. A simple two-phase frictional pressure drop calculation method. International Journal of Multiphase Flow 8, 83–87.

Chen, I., Wang, C.-C., Lin, S., 2004. Measurements and correlation of frictional single-phase and two-phase pressure drops of R-410A flow in small U-type return bends. Experimental Thermal and Fluids Science 47, 2241–2249.

Chen, I., Wu, Y.-S., Chang, Y.-J., Wang, C.-C., 2007. Two-phase frictional pressure drop of R-134a and R-410A refrigerant-oil mixtures in straight tubes and U-type wavy tubes. Experimental Thermal and Fluids Science 31, 291–299.

Chen, I., Wu, Y.-S., Liaw, J.-S., Wang, C.-C., 2008. Two-phase frictional pressure drop measurements in U-type wavy tubes subject to horizontal and vertical arrangements. Applied Thermal Engineering 28, 847–855.

Chisholm, D., 1980. Two-phase flow in bends. International Journal of Multiphase Flow 6, 363–367.

Chisholm, D., 1983. Two-phase flow in pipelines and heat exchangers. George Godwin, London.

Chisholm, D., Sutherland, L., 1969. Prediction of pressure gradients in pipeline systems during two-phase flow. International Journal of Multiphase Flow 184(3), 24–32.

da Silva Lima, R., Thome, J., 2012. Two-phase flow patterns in U-bends and their contiguous straight tubes for different orientations, tube and bend diameters. International Journal of Refrigeration 35(5), 1439–1454.

da Silva Lima, R., Thome, J., 2013. Two-phase flow pressure drops in U-tubes: Towards more accurate measurement methods and prediction models. International Journal of Refrigeration 36(2), 492–503.

De Kerpel, K., De Keulenaer, T., De Schampheleire, S., De Paepe, M., 2014. Capacitance sensor measurements of upward and downward two-phase flow in vertical return bends. International Journal of Multiphase Flow 64, 1–10.

De Kerpel, K., De Schampheleire, S., De Keulenaer, K., De Paepe, M., 2016a. Two-phase frictional pressure drop and flow behaviour up- and downstream of a sharp return bend. Applied Thermal Engineering 93, 824–838.

De Kerpel, K., De Schampheleire, S., De Keulenaer, T., De Paepe, M., 2016b. Effect of the bend geometry on the two-phase frictional pressure drop and flow behaviour in the vicinity of the bend. Applied Thermal Engineering 104, 403–413.

de Oliveira, P., Barbosa, J., 2014. Pressure drop and gas holdup in air–water flow in 180° return bends. International Journal of Multiphase Flow 61, 83–93.

de Oliveira, P., Strle, E., Barbosa, J., 2014. Developing air–water flow downstream of a vertical 180° return bend. International Journal of Multiphase Flow 67, 32–41.

Domanski, P., Hermes, C., 2008. An improved correlation for two-phase pressure drop of R-22 and R410A in 180° return bends. Applied Thermal Engineering 28, 793–800.

Geary, D., 1975. Return bend pressure drop in refrigeration systems. ASHRAE Transactions 81(1), 250–265.

Idelchik, I., 1986. Handbook of Hydraulic Resistance, 2nd Edition. Hemisphere, New York.

Lockhart, R. W., Martinelli, R. C., 1949. Proposed correlation of data for isothermal two-phase, two-component flow in pipes. Chemical Engineering Progress 45, 38–48.

Mandal, S., Das, S., 2001. Pressure losses in bends during two-phase gas-newtonian liquid. Industrial & Engineering Chemistry Research 40, 2340–2351.

Muller-Steinhagen, H., Heck, K., 1986. A simple friction pressure drop correlation for two-phase flow in pipes. Chemical Engineering and Processing 20, 297–308.

Padilla, M., Revellin, R., Bonjour, J., 2009. Prediction and simulation of two-phase pressure drop in return bends. International Journal of Refrigeration 32, 1776–1783.

Padilla, M., Revellin, R., Bonjour, J., 2012. Two-phase flow visualization and pressure drop measurements of HFO-1234yf and R-134a refrigerants in horizontal return bends. Experimental Thermal and Fluid Science 39, 98–111.

Padilla, M., Revellin, R., Wallet, J., Bonjour, J., 2013. Flow regime visualization and pressure drops of HFO-1234yf, R-134a and R-410A during downward two-phase flow in vertical return bends. International Journal of Heat and Fluid Flow 40, 116–134.

Sekoguchi, K., Sato, Y., Kariyazaki, S., 1969. Horizontal to-phase air-water flow characteristics in a disturbed region due to 90o bends. Transaction of the Japanese Society of Mechanical Engineers 35(279), 2227–2233.

Tay, B. L., Thorpe, R. B., 2014. Hydrodynamic forces acting on pipe bends in gas-liquid slug flow. Chemical Engineering Research and Design 92, 812–825.

Traviss, D., Rohsenow, W., 1973. Horizontal to-phase air-water flow characteristics in a disturbed region due to 90o bends. In: Proceedings of ASHRAE Semiannual Meeting. Chicago, pp. 2269RP–63.

Wang, C. C., Chen, I. Y., Shyu, H. J., 2003. Frictional performance of R-22 and R-410A inside a 5.0 mm wavy diameter tube. International Journal of Heat and Mass Transfer 46, 755–760.